ASSOCIAZIONE NAZIONALE ITALIANA DI INGEGNERIA SISMICA
ANIDIS
Italian National Association of Earthquake Engineering

XVIII CONVEGNO ANIDIS
L'ingegneria sismica in Italia
ASCOLI PICENO 2019
15-19 Settembre

Out-of-Plane fragility of infill walls with and without prior in-plane damage

Fabio Di Trapani[a], Sara Cirelli[a], Gabriele Bertagnoli[a], Marzia Malavisi[a], Marco Filippo Ferrotto[b]
[a] *Dipartimento di Ingegneria Strutturale, Edile e Geotecnica, Politecnico di Torino, Corso Duca degli Abruzzi 24, 10129, Turin, Italy*
[b] *Dipartimento di Ingegneria, Università degli Studi di Palermo, Viale della Scienze, 90128, Palermo, Italy*

Keywords: Incremental Dynamic Analysis, Fragility Curves, Masonry Infilled Frames, Reinforced concrete

ABSTRACT
The paper presents the results of a probabilistic assessment framework aimed at evaluating out-of-plane fragility curves of infill walls which have suffered (or not) prior in-plane damage. Out-of-plane incremental dynamic analyses are performed based on a suite of 26 ground motion records. A recently developed in-plane / out-of-plane macro-element model is used to model masonry infills within frames. The outcomes show fragility curves representing the probability of exceeding out-of-plane collapse at a given earthquake intensity as a function of a different combination of geometrical and mechanical parameters, in-plane damage level and supporting conditions.

1 INTRODUCTION

In the last years, the out-of-plane (OOP) earthquake response of masonry infills and its mutual dependence with the in-plane (IP) damage level has received special interest by researchers. New experimental investigations (e.g. Furtado et al. 2016, Ricci et al. 2018, De Risi et al. 2019) have been carried out and, at the same time, new simplified models able to predict both in-plane and out-of-plane responses have been developed following different mechanical approaches. Among these, the models by Mosalam and Günay 2014, Furtado et al. 2015, Di Trapani et al. 2018a were formulated using the OpenSEES software platform (McKenna et al. 2000) and thus represent a tool for more complex simulations.

The response of masonry infilled reinforced concrete (RC) frame buildings subject to ground motions inducing in-plane and out-of-plane actions is not of easy generalization as this depends on several aspects as the geometrical configuration of the frame, the position of the infills along the height, the reciprocal earthquake intensity along the two orthogonal directions. Some recent studies referred to the analysis entire buildings (Ricci et al. 2019, Longo et al. 2019) have confirmed this. In fact, infills located at the highest floor are subjected to major accelerations but at the same time lower in-plane damage. On the contrary, infills at the lowest floors undergo reduced accelerations demand but suffer large in-plane drift demand that waken their out-of-plane capacity. The issues is made more complicated by the record-to-variability associated with the ground motions and by the arbitrariness of their direction of action. Considering these premises, a prediction of the most critical conditions for the infill walls in a frame structure cannot be carried in a simple way in case of combined IP-OOP actions.

In this paper the issue is faced using a probabilistic assessment framework aimed at evaluating out-of-plane fragility curves of infill walls which have been subjected (or not) prior in-plane damage. The fiber-section macro-element model by Di Trapani et al. (2018a) is used to model the infill wall. Fragility curves are obtained performing out-of-plane incremental dynamic analyses (IDA) based on a suite of 26 ground motion records. IDA curves, and the associated fragilities are obtained by varying the slenderness ratio, the in-plane drift level, and the frame stiffness with respect to the out-of-plane stiffness of the infill. The final output consist of a set of curves, representing the average peak ground acceleration (PGA) inducing the collapse of the infill, as a function of the aforementioned design

variables, considering also the altitude of an infill with respect to the total height of the building.

2 IP-OOP MACRO-MODEL AND ITS ADAPTION TO DYNAMIC ANALYSIS

2.1 Description of the macro-element model

The macro-element model by Di Trapani et al. (2018a) provides the replacement of the infill panel with 4 pinned struts, each one divided into two elements. The overall scheme is illustrated in Fig. 1.

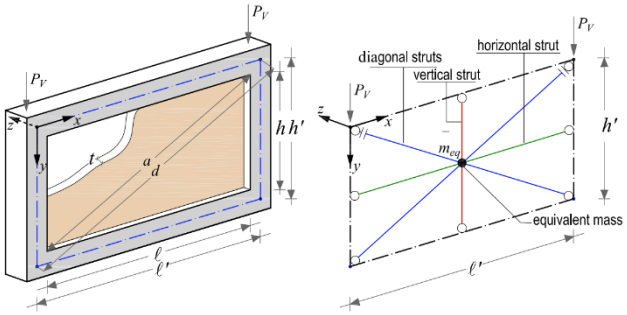

Figure 1. Geometrical definition of the 4-strut macro-model.

Each strut is defined using distributed plasticity fiber-section beam-column elements available in OpenSEES. In this way, internal cross-section forces of these elements are related to the corresponding deformations (axial deformation and curvature), hence, after the elastic stage axial load is coupled with bending moment and the arching mechanism is then naturally accounted. The diagonal, horizontal and vertical struts have typical concrete-type stress-strain laws, modelled with the OpenSEES Concrete02 material (Fig. 2). In the current study, in order to consider more explicitly the effects of the strength degradation, the Concrete02 material model is combined with the MinMax material so that, once the ultimate strain is attained at a generic fiber, the corresponding stress drops to zero. The diagonal struts are constrained with pins at the ends. They provide the whole in-plane response of the infill as well as the main OOP contribution. The horizontal and vertical struts provide a complementary OOP contribution to strength, reproducing the 2-way bending effect of the panel. The 4 struts do not share the mid-span node but are constrained to move together along the z direction. In this way each strut can provide its strength contribution to the OOP response. Geometrical and mechanical identification of the struts is performed starting from the diagonals, whose force-displacement behaviour can be assigned by adopting any method. Once that the force-displacement law is determined, this can be easily converted into an equivalent concrete-type stress-strain relationship and assigned to the cross-section fibers.

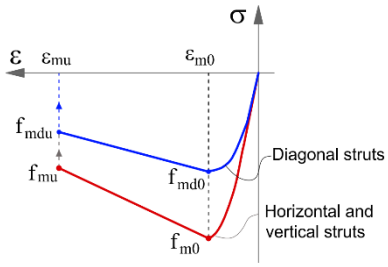

Figure 2. Geometrical definition of the 4-strut macro-model.

To perform this step, the reference cross-section can be simply obtained by fixing the width (w_d) as 1/3 of the internal diagonal length (a) and the thickness as the actual thickness (t) of the infill. A direct definition of the stress-strain relationship and width of the diagonal cross-sections can also performed following the approach by Di Trapani et al. (2018b). When defining the stress-strain relationship of the diagonal struts it can be easily found that the peak strength f_{md0} is lower than the actual compressive strength of masonry (f_{m0}). This is due to the fact that the strength f_{md0} expresses a fictitious resistance summarizing the complex response of the infill subject to lateral forces. On the other hand, the out-of-plane strength is proportional to the actual compressive strength of the masonry (f_{m0}), therefore, the out-of-plane contribution offered by the diagonals results underestimated as a consequence of the adoption of strength f_{md0}. In order to compensate this drawback, the cross-section thickness is increased by the ratio f_{m0}/f_{md0} as follows:

$$\tilde{t} = \frac{f_{m0}}{f_{md0}} t \tag{1}$$

while, in order to maintain unaltered the cross-section area, the width is reduced as:

$$\tilde{w}_d = \frac{t}{\tilde{t}} w_d \tag{2}$$

The residual OOP strength is provided by the horizontal and vertical struts. The latter are defined using the actual thickness t of the infill and the actual strength f_{m0}, while the widths are obtained as the difference between the height and the length of the panel and the horizontal and vertical projections of the diagonal initial width w_d on the infill perimeter. The widths of the horizontal strut (w_h) and vertical strut (w_v) are therefore evaluated as follows (Fig. 3):

$$w_h = h - \frac{w_d}{\cos\theta}; \quad w_v = \ell - \frac{w_d}{\sin\theta} \tag{3}$$

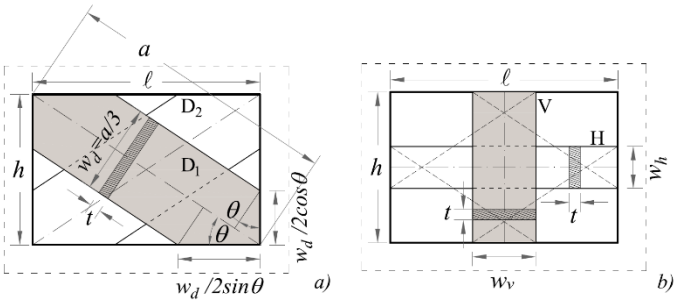

Figure 3. Identification of the dimensions of the horizontal and vertical struts: a) definition of the projection of the diagonals; b) definition of the cross-section dimensions.

2.2 *Determination of the equivalent mass*

In order to perform dynamic simulations, an equivalent mass to apply at the midspan node of the model has to be defined. The mass (m_{eq}) of the so defined single degree of freedom (SDOF) system will be a percentage of the total mass of the infill. In order to identify this percentage, an experimental/numerical identification procedure has performed using the results of the experimental tests by Angel (1994), which were also used for the validation of the aforementioned model. The tests regarded reinforced concrete infilled frame specimens subject to in-plane cycles and then pushed out-of-plane using an airbag. The identification procedure consists of the following steps: *a*) determination of the experimental out-of-plane stiffness (K_{exp}) from the experimental force-displacement diagrams; *b*) identification of the out-of-plane period of the infill ($T_{i,FEM}$) by defining an elastic finite element model of a plate pinned at the sides (Fig. 4), verifying that the stiffness of the plate (K_{FEM}) was the same as the experimental stiffness; *c*) determination of the equivalent mass of the SDOF system as:

$$m_{eq} = \frac{T_{i,FEM}^2}{4\pi^2} K_{exp} \quad (4)$$

In the procedure it is assumed that the out-of-plane stiffness provided by the macro-model is the same as that the experimental stiffness. This was proved in the validation tests by Di Trapani et al. (2018a) for the same specimens. It should be also observed that that since the specimen were subjected to moderate cycles before being tests out-of-plane, their experimental stiffness were lower with respect to that estimated by the elastic FE model of the plate. Therefore, the matching between K_{FEM} and K_{exp} was obtained by modifying the elastic modulus of the infill (E_m) into a lower one (E_m^*). This manipulation has no influence on the equivalent mass value found by Eq. (4), with respect to an undamaged case, since the reduction of K_{FEM} due to the reduction of E_m in the FE model, is compensated by the elongation of the period. Geometric dimensions and masses of the infills of specimens by Angel (1994) are reported in Table 1. Mechanical properties of the infills are reported in Table 2 together with the obtained experimental stiffness values, periods and equivalent masses. It is noteworthy observing that independently on the different geometric and mechanical combinations of the specimens the percentage equivalent mass resulted 55% of the total mass on average. This allows concluding that the macro-element model can be adapted to perform dynamic simulations by assigning a 55% equivalent mass at the central node.

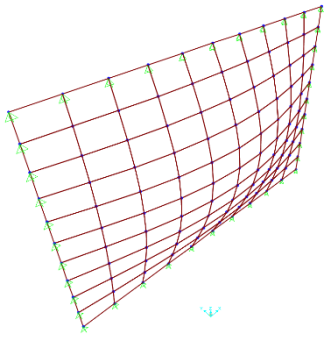

Figure 4. First modal shape of the FE model of the infill.

Table 1. Geometric dimensions and masses of specimens by Angel (1994).

Spec.	ℓ (mm)	ℓ' (mm)	h (mm)	h' (mm)	t (mm)	h/t (-)	γ (kN/m^3)	mass (kg)
2	2440	2740	1630	1930	47.6	34.2	19	359.7
3	2440	2740	1630	1930	47.6	34.2	19	359.7
4	2440	2740	1630	1930	92.0	17.7	19	695.2
5	2440	2740	1630	1930	143.0	11.4	19	1080.6
6	2440	2740	1630	1930	98.4	16.6	19	743.6

Table 2. Mechanical properties and identification parameters of specimens tested by Angel (1994).

Spec.	E_m (MPa)	G_m (MPa)	E_m^* (MPa)	f_{m0} (MPa)	K_{exp} (N/mm)	$T_{i,FEM}$ (s)	m_{eq} (kg)	$m_{eq\%}$ (%)
2	8040	8040	1900	10.85	1052.6	0.083	184.5	51.3
3	5208	5208	1736	10.13	1300	0.078	202.3	56.2
4	12429	12429	5000	22.90	20000	0.027	364.2	52.4
5	11616	11616	9000	22.82	148000	0.012	582.6	53.9
6	2136	2136	650	4.60	3500	0.070	429.0	57.7

3 ANALYSIS FRAMEWORK FOR THE ONE-STOREY INFILLED FRAME

3.1 *Definition of the analysis program*

The investigation is first aimed at deriving out-of-plane fragility curves of a one-storey infilled frame as a function of different conditioning boundary conditions, namely the slenderness ratio and strength of the specimen, the extent of the previous in-plane damage, the out-of-plane vibration period of the infill with respect to that of the supporting frame structure. Two reference

specimens among those tested by Angel (1994) have been selected to perform fragility assessment, namely Specimen 2 and Specimen 6. These specimens have different slenderness ratios and masonry strength as it can be observed from Tables 1 and 2. The OOP resistance of these infills (F_r) can be estimated through the EC6 expression as:

$$F_r = f_{m0}\left(\frac{t}{h'}\right)^2 \ell h \tag{5}$$

From Eq.(5) one can determine the OOP resisting pressure (f_r) as:

$$f_r = \frac{F_r}{\ell h} \tag{6}$$

which is used as parameter to classify a class of infills. For specimens 2 and 6 f_r is 6.6 MPa and 11.95 MPa respectively. In order to simulate the influence of the supporting frame, the reference infilled frame is modelled as in Fig. 5, where besides the equivalent mass at the midspan node, the model presents 4 mass-spring (m_f ,k_f) systems at the corner nodes. The whole system has finally two degrees of freedom, one related to the frame, the other related to the infill. The vibration period associated with the frame considered alone can be evaluated as:

$$T_f = 2\pi\sqrt{\frac{M_f}{K_f}} \tag{7}$$

in which $M_f=4m_f$ is the total mass of the frame $K_f=4k_f$ is the total stiffness of the parallel springs, while the vibration periods associated with the infills (T_i) have been defined in the previous section. The springs have elastic behaviour and are modelled in OpenSEES using zero-length elements. For the two specimens under investigation, the response of the system is analyzed considering five different supporting conditions, namely rigid support ($K_f=\infty$), $T_f=T_i$, $T_f=3T_i$, $T_f=5T_i$, $T_f=7T_i$. Given that the period of the infills is fixed, and attributing a conventional mass (m_f) of 2000 kg to the nodes of the frames, the stiffness of the frame producing the aforementioned period ratios can be obtained as:

$$K_f = 4\pi^2\frac{M_f}{T_f^{\,2}} \tag{8}$$

and then:

$$k_f = 4\pi^2\frac{m_f}{T_f^{\,2}} \tag{9}$$

The effect of prior in-plane damage is also investigated considering 4 cases, namely: a) no in-plane damage; b) IDR=0.5%; c) IDR=1.5%; d) IDR=2.5% (Fig. 6). The IDR (interstorey drift) is used as measure of the in plane damage. The analyses are carried out in OpenSEES in two-steps. First a cyclic static analysis consisting of three cycles having amplitude as the fixed IDR is performed. Subsequently the IDA sequence is started. A summary of the analyses is reported in Table 3. Details about periods, and stiffness of the different systems obtained for Specs. 2 and 6 are listed in Tables 4 and 5.

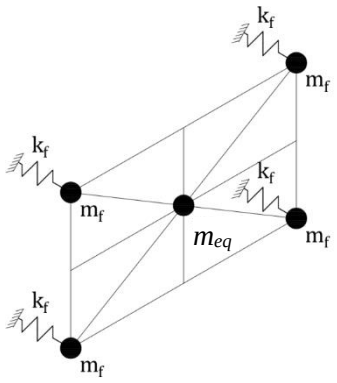

Figure 5. Reference scheme of the infilled frame model.

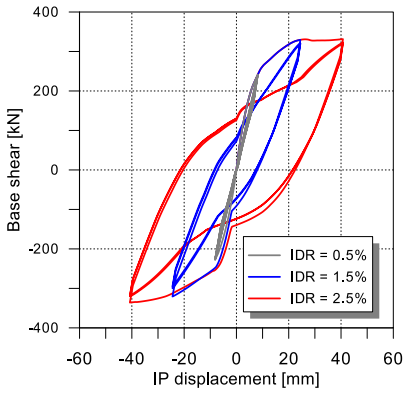

Figure 6. IP response of Spec. 2 to different drift levels.

Table 3. Summary of the test conditions.

Support conditions	**Specimen 2**	**Specimen 6**
	IDR (%)	**IDR (%)**
T_f=0 (Rigid frame)	0 / 0.5 / 1.5 / 2.5	0 / 0.5 / 1.5 / 2.5
$T_f=T_i$	0 / 0.5 / 1.5 / 2.5	0 / 0.5 / 1.5 / 2.5
$T_f=3T_i$	0 / 0.5 / 1.5 / 2.5	0 / 0.5 / 1.5 / 2.5
$T_f=5T_i$	0 / 0.5 / 1.5 / 2.5	0 / 0.5 / 1.5 / 2.5
$T_f=7T_i$	0 / 0.5 / 1.5 / 2.5	0 / 0.5 / 1.5 / 2.5

Table 4. Period, mass and stiffness values of the systems obtained by Spec. 2

T_f/T_i	T_i	T_f	M_f	K_f	k_f
(-)	(s)	(s)	(kg)	(kN/m)	(kN/m)
0	0.083	0	8000	∞	∞
1	0.083	0.083	8000	3801.3	950.3
3	0.083	0.249	8000	1267.1	316.8
5	0.083	0.415	8000	760.3	190.1
7	0.083	0.581	8000	543.0	135.8

Table 5. Period, mass and stiffness values of the systems obtained by Spec. 6

T_f / T_i	T_i	T_f	M_f	K_f	k_f
(-)	(s)	(s)	(kg)	(kN/m)	(kN/m)
0	0.07	0	8000	∞	∞
1	0.07	0.07	8000	4507.2	1126.8
3	0.07	0.21	8000	1502.4	375.6
5	0.07	0.35	8000	901.4	225.4
7	0.07	0.49	8000	643.9	161.0

3.2 Definition of out-of-plane IDA curves

Incremental Dynamic Analysis (IDA) (Vamvatsikos and Cornell, 2002) has been carried out using the peak ground acceleration (PGA) as intensity measure (IM) and the out-of-plane net displacement (Δ_{OOP}) as damage measure (DM). 26 ground motions records have been considered. The spectra of the selected ground motion are illustrated in Fig. 7. The choice of PGA as IM instead of the usual spectral acceleration in correspondence of the first vibration period is due to the fact that, as explained in the previous section, different combinations of periods are considered. The choice of PGA allows using the same ground motion scaling the to analyse the different combinations of periods. In detail the ground motions are first scaled so that their respective spectra have the same PGA. The subsequent scaling during IDA uniformly increases / decreases the amplitude. For each ground motion IDA are stopped in correspondence of the achievement of dynamic instability, which represents the OOP failure of the infill. After this point, a constant flatline is conventionally represented.

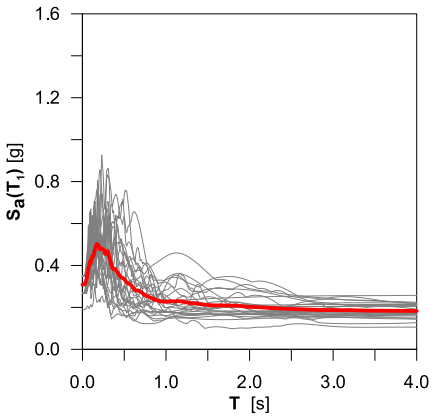

Figure 7. Reference scheme of the infilled frame model.

3.3 Definition of out-of-plane fragility curves

Fragility curves express the probability of exceeding a specified limit state as a function of the specified IM (PGA). Fragility curves can be represented using a lognormal cumulative distribution function as:

$$P[C \le D \mid IM = x] = \Phi\left(\frac{ln(x) - \mu_{ln_x}}{\sigma_{ln_x}}\right) \quad (10)$$

where $P[C \le D \mid IM = x]$ is the probability that a ground motion with IM=x will cause the achievement of a limit state, Φ is the standard cumulative distribution function, $ln(x)$ is the natural logarithm of the variable x representing the intensity measure (PGA) and μ_{lnX} and σ_{lnX} are the mean and the standard deviation of the natural logarithms of the distribution of x, respectively.

Fragility curves are derived considering the collapse limit state, which is attained when the dynamic instability occurs during IDA or when the midspan relative displacement of the infill (Δ_{OOP}) is the same as the thickness of the infill. In this latter case, in fact, it is supposed that the aching action vanishes and the equilibrium is lost.

Cumulative discrete distribution functions are also overlapped to the analytically obtained fragility curves to verify the adequacy of the distribution model.

4 RESULS OF THE ANALYSIS ON THE ONE-STOREY INFILLED FRAME

4.1 IDA curves

IDA curves are illustrated in Fig. 8-11 for the one-storey infilled frame for different considered combinations of T_f/T_i ratio and in-plane IDR. For sake of space, IDA curves are only shown for specimen 2. The curves show a reduction of the average collapse PGA when increasing T_f/T_i up to 3. After the collapse PGA tends to increase again, denoting that T_f/T_i ratio has a relevant role, as it influences the accelerations experienced by the infill wall. On the other hand, it should be also observed that the presence of in-plane damage (measured by the in-plane IDR) tends to reduce the influence of T_f/T_i. In fact in presence of severe damage (IDR=1.5.%-2.5%) the collapse PGA is dramatically reduced. Under these conditions no substantial differences can be observed when varying T_f/T_i ratio.

4.2 Fragility curves

Fragility curves of the one-storey infilled frame are shown in Fig. 12. The latter reflect what already observed form IDA curves. For the case of no-IP damage and moderate IP damage (IDR=0.5%) (Figs. 12a-12b) fragility tends to

increase when increasing T_f/T_i up to 3. After this point fragility tends to be reduced, although significantly larger dispersion of collapse IMs is observed. For the cases of high IP damage (Figs. 12a-12b) fragility curves result significantly shifted on the right denoting minor sensitivity to variation of T_f/T_i. In some cases, PGA values may result very high, so that they can exceed collapse PGA of the frame.

It should be anyway observed that results are referred to the one-storey infilled frame which suffers moderate floor accelerations. In the next section the investigation will be extended to the case of multi-storey frame under the simplified assumption of linear distribution of floor accelerations.

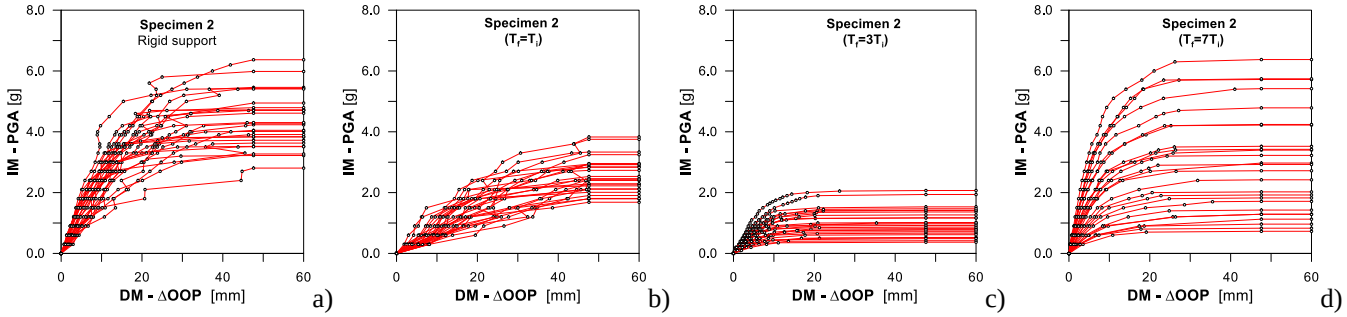

Figure 8. IDA curves of Specimen 2 without in-plane damage for: a) rigid support; b) $T_f=T_i$; b) $T_f=3T_i$; b) $T_f=7T_i$.

.

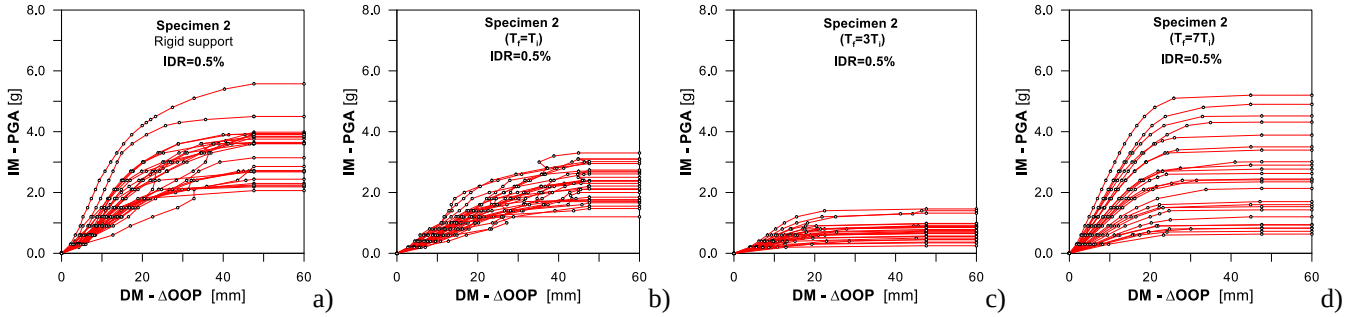

Figure 9. IDA curves of Specimen 2 with IDR=0.5% for: a) rigid support; b) $T_f=T_i$; b) $T_f=3T_i$; b) $T_f=7T_i$.

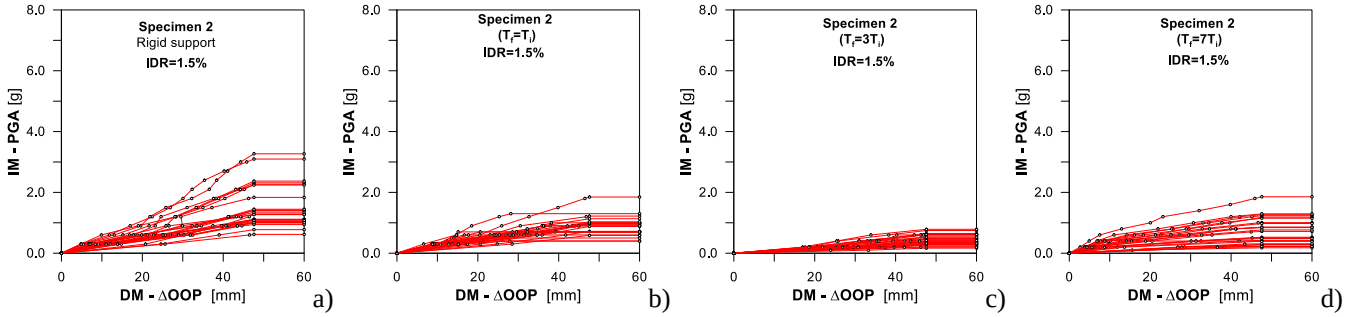

Figure 10. IDA curves of Specimen 2 with IDR=1.5% for: a) rigid support; b) $T_f=T_i$; b) $T_f=3T_i$; b) $T_f=7T_i$.

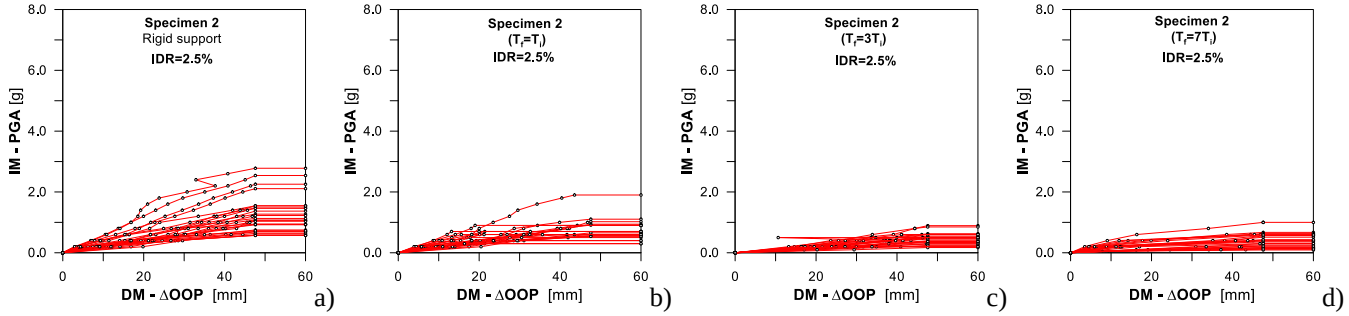

Figure 11. IDA curves of Specimen 2 with IDR=2.5% for: a) rigid support; b) $T_f=T_i$; b) $T_f=3T_i$; b) $T_f=7T_i$.

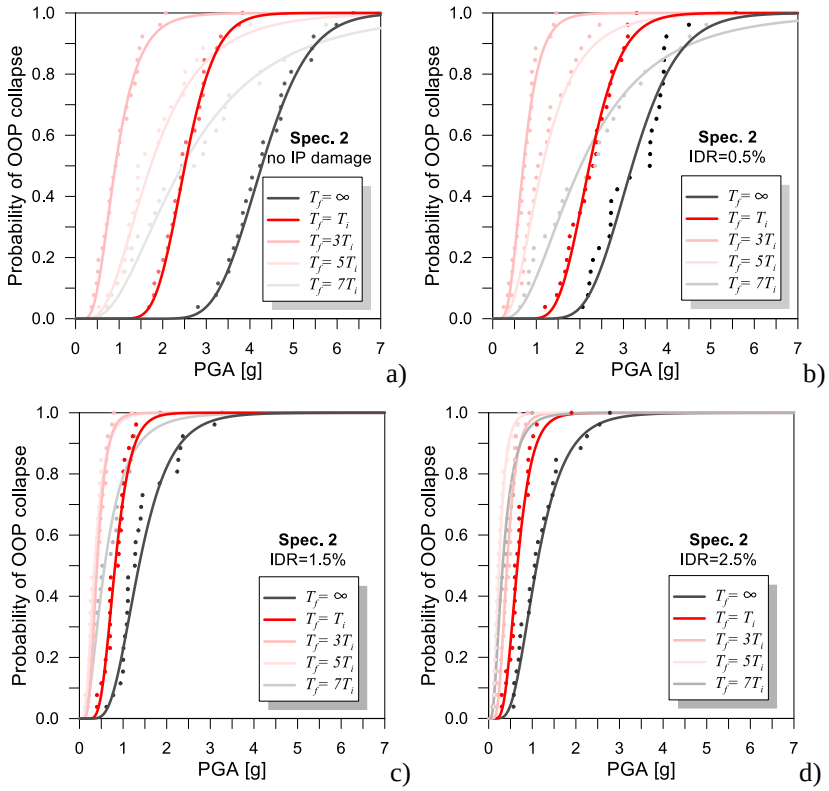

Figure 12. Fragility curves of specimen 2 for different T_f/T_i with: a) IDR=0 %; b) IDR=0.5 %; c) IDR=1.5 %; d) IDR=2.5 %.

5 EXTENSION OF RESULTS TO MULTI-STOREY INFILLED FRAMES

Results shown in the previous section are referred to the elementary one-storey infilled frame, which is supposed to be subjected to an acceleration history at the supports. In the case of a multi-storey frame, floor accelerations tend to grow when increasing the height, as also provided by EC6 through the expression:

$$S_a = PGA \cdot S \cdot \beta \tag{11}$$

where S is the soil factor, S_a the pseudo acceleration of an infill wall at the center of mass, positioned at the altitude (Z) from the ground in a building having total height (H) and β is a modulation coefficient so defined:

$$\beta = \frac{3(1+Z/H)}{1+(1-T_i/T_f)^2} - 0.5 \tag{12}$$

It is easy to demonstrate that according to Eq. (11) S_a increases with increasing the altitude of the infill with respect to the total height of the building, according to a linear relationship. Moreover, given that the effect of the variation of the ratio between T_f and T_i has been already taken into account in the previous analysis of the one-storey infilled frame, in Eq. (12) it can be set $T_i/T_f=0$. Finally, for consistency with the assumed scheme for the one-storey infilled frames, the values Z' and H' are used instead of Z and H, where Z' is the quote of the center of mass of the infill measured with respect to the center of mass of the first ground floor infill, and H' is the quote of the center of mass of the infill at the highest floor. Under this assumptions one obtains:

$$\beta^* = \frac{3(1+Z'/H')}{2} - 0.5 \tag{13}$$

It can be easily observed that if $Z'/H'=0$ (case of infill wall at the ground floor or one storey infilled frame), $\beta^*=1$ (no amplification is provided), while If $Z'/H'=1$ (case of infill wall at the top floor) one obtain the maximum amplification factor ($\beta^*=2.5$).

By defining $\overline{PGA}_{C,0}$ as the 50% probability PGA inducing the collapse of the one-storey infilled frame, it can be recognized that the average PGA inducing the collapse of an infill wall at the generic Z/H position ($\overline{PGA}_{C(Z/H)}$) can be obtained by reducing $\overline{PGA}_{C,0}$ by β^* as follows:

$$\overline{PGA}_{C(Z/H)} = \frac{\overline{PGA}_{C,0}}{\beta^*} \tag{14}$$

The values of $\overline{PGA}_{C,0}$ are extrapolated from the fragility curves and represented as in Figs. 13a and 14a for specimens 2 and 6 respectively. This are coincident with $\overline{PGA}_{C(Z/H)}$ at $Z'/H'=0$. Diagrams in Figs. 13b-c and 14b-c represent $\overline{PGA}_{C(Z/H)}$ for $Z'/H'=0.5$ and $Z'/H'=1$. The latter are obtained from the first two diagrams by using Eq. (14).

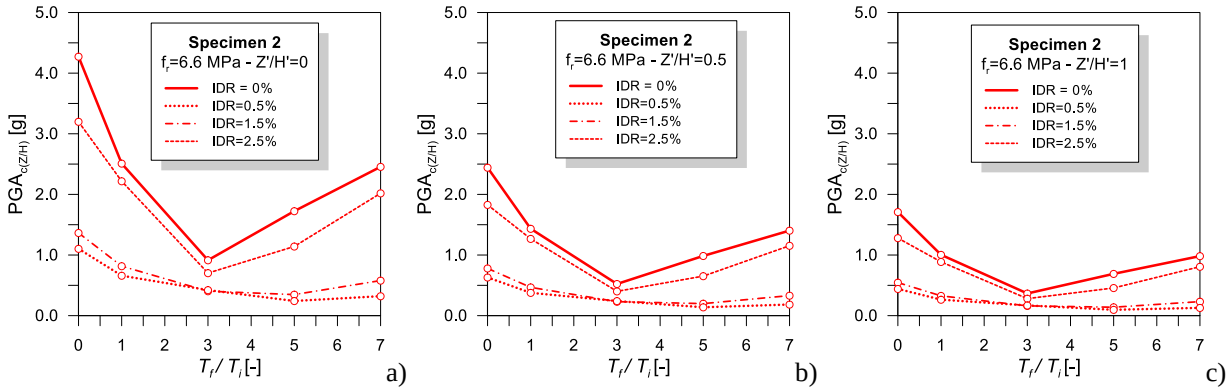

Figure 13. Average collapse PGA for Specimen 2 with: a) Z'/H'=0; a) Z'/H'=0.5; c) Z'/H'=1.0.

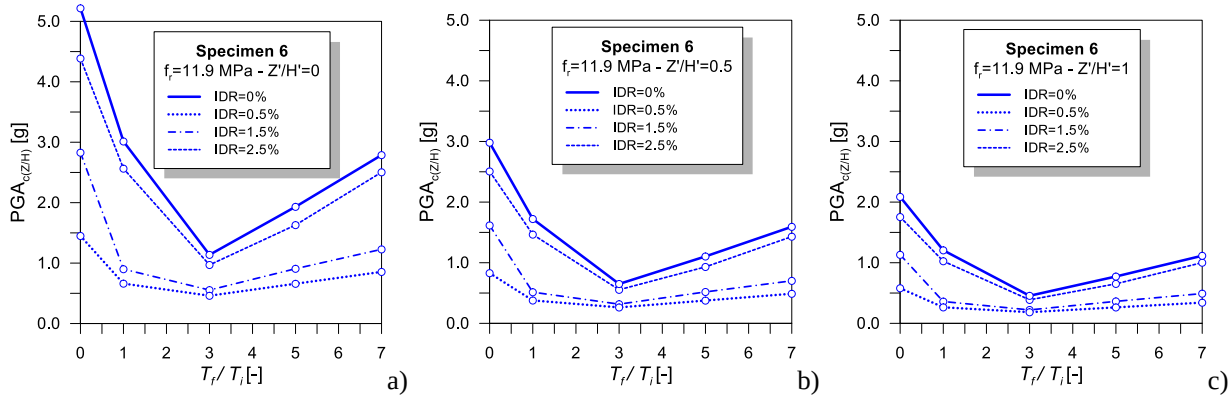

Figure 14. Average collapse PGA for Specimen 6 with: a) Z'/H'=0; a) Z'/H'=0.5; c) Z'/H'=1.0.

Diagrams in Figs. 13-14 show that infill at the higher stories undergo major spectral acceleration and therefore their collapse may occur with significantly reduced PGA levels. At the same time infills positioned at lower stories suffer major in-plane damage and therefore their collapse may anticipate collapse of infills at upper stories.

6 CONCLUSIONS

In the paper an existing infilled frame macro-element model (Di Trapani et al. 2018a) has been updated to perform dynamic simulations. The paper consist of four fiber-section struts and is able to account for mutual in-plane and out-of-plane damage. Out-of-plane fragility curves for a reference one-storey infilled frames have been derived considering different prior IP damage levels and different ratios between frame and infill periods (T_f/T_i). Incremental dynamic analysis was used to derive fragility curves. Results have shown that for the cases of no-IP damage and moderate IP damage the average collapse PGA tend to increase when increasing T_f/T_i up to 3. After this point collapse PGA tends to be reduced. For the cases of high IP damage collapse PGA dramatically decreases denoting minor sensitivity to T_f/T_i. The analysis has been extended to multi storey infilled frames under the simplified assumption of linear distribution for floor accelerations. It has been shown that infills at the higher stories undergo major spectral acceleration and their collapse may be achieved in correspondence of reduced PGA values. However infills positioned at lower stories undergo major in-plane damage potentially causing their anticipated collapse with respect to the upper stories infills. In conclusion, the location of masonry infills subject to major OOP collapse risk in not predictable a priori as this depends on the combination between floor acceleration and in-plane drift at each storey.

REFERENCES

Angel, R., 1994. Behavior of reinforced concrete frames with masonry infill walls. PhD thesis, *University Illinois at Urbana-Champaingn*, Illinois, USA.

De Risi, M.T., Di Domenico, M., Ricci, P., Verderame, G.M., Manfredi, G., 2019. Experimental investigation on the influence of the aspect ratio on the in-plane/out-of-plane interaction for masonry infills in RC frames, *Eng Struct*, **189**, 523–540.

Di Trapani, F, Shing, P.B., Cavaleri, L., 2018a. Macroelement model for in-plane and out-of-plane responses of masonry infills in frame structures, *J Struct Eng*, **144**:04017198.

Di Trapani, F., Bertagnoli, G., Ferrotto, M.F., Gino, D., 2018b. Empirical equations for the direct definition of

stress-strain laws for fiber-section based macro-modeling of infilled frames, *J Eng Mech*, **144**(11): 04018101.

Eurocode 6. Design of Masonry Structures. Part 1-1: General Rules for Reinforced and Unreinforced Masonry Structures. Brussels, 2005.

Furtado, A., Rodrigues, H., Arêde, A., Varum, H., 2015. Simplifed macro-model for infll masonry walls considering the out-of-plane behaviour, *Earthq Eng Struct Dyn* **45**(4), 507-524.

Furtado, A., Rodrigues, H., Arêde, A., Varum, H., 2016. Experimental evaluation of out-of-plane capacity of masonry infill walls, *Eng Struct*, **111**, 48–63

Longo, F., Wiebe, L., da Porto, F., Modena, C., 2018. Application of an in plane/out of plane interaction model for URM infill walls to dynamic seismic analysis of RC frame buildings, *Bull Earthquake Eng*, **16**, 6163-6190.

McKenna, F., Fenves, G.L., Scott, M.H., 2000. Open system for earthquake engineering simulation. University of California, Berkeley.

Mosalam, K.M., Günay, S., 2015. Progressive collapse analysis of RC frames with URM infill walls considering in-plane/out-of-plane interaction, *Earthq Spectra*, **31**(2), 921-943.

Ricci, P., Di Domenico, M., Verderame, G.M., 2018. Experimental assessment of the in-plane/out-of-plane interaction in unreinforced masonry infill walls, *Eng Struct*, **173**, 960–978

Ricci, P., Di Domenico, M., Verderame, G.M., 2019. Out-of-plane seismic safety assessment of URM infills accounting for the in-plane/out-of-plane interaction in a nonlinear static framework, *Eng Struct* **195**, 96–112.

Vamvatsikos, D., Cornell, A.C., 2002. Incremental dynamic analysis. *Earthq Eng Struct Dyn*, **31(3)**, 491–514.